

**THE COMPOSITION AND SPECIATION OF COHS FLUIDS IN SUBDUCTED
(CONTINENTAL) MARBLES: COMPARATIVE INSIGHTS FROM FLUID
INCLUSIONS AND THERMODYNAMICS.
A CASE STUDY FROM THE UHP MARBLES OF THE DORA-MAIRA MASSIF**

MAFFEIS ANDREA

Dipartimento di Scienze della Terra, Università di Torino, Via Valperga Caluso 35, 10125 Torino

INTRODUCTION

Carbon and Sulphur are two of the most influential elements on both the short-term and long-term evolution of multiple Earth domains, from the biosphere to the atmosphere and hydrosphere down to the lithosphere. They make possible life itself and regulate climate on Earth on a geologic scale (long term: 10^6 years) via their continuous flux between surficial and deep reservoirs. Moreover, both elements play a crucial role in the redox evolution of the lithospheric mantle, which regulates the speciation of COH(S) fluids and melts and, ultimately the mantle solidus and the properties of resulting liquids (*e.g.*, Taylor & Green, 1988; Ballhaus & Frost, 1994; Frost & McCammon, 2008). Subduction zones play a key role in delivering C and S from the surficial reservoirs down within the Earth (Plank & Manning, 2019). Both S and C can be dissolved in seawater and are incorporated in oceanic sediments and crust before being recycled into the mantle (Kagoshima *et al.*, 2015), where they can be either stored, respectively, as carbonate/diamond and as sulphides (*e.g.*, Malusà *et al.*, 2018) for 10^5 to 10^8 years. In hot subduction zones, C and S can be transferred to the mantle wedge by ascending melts from the down-going slab. On the contrary, in colder subduction zones, where slab melting is inhibited at subarc depths, C and S can be effectively mobilised aqueous fluids as dissolved CO_2 , $\text{CO}_3^{2-}/\text{HCO}_3^-$, carboxylic compounds and hydrocarbons and as SO_4^{2-} , other S oxyanions, polysulphides, S_3^- radicals and $\text{H}_2\text{S}/\text{HS}^-$, respectively (*e.g.*, Frezzotti *et al.*, 2011; Sverjensky *et al.*, 2014; Facq *et al.*, 2014; Galvez *et al.*, 2016; Frezzotti, 2019; Huang & Sverjensky, 2019; Walters *et al.*, 2020; Li *et al.*, 2021). Pressure, temperature and $f\text{O}_2$ are the controlling factors that decide whether such fluids will have the chemical-physical (*i.e.*, speciation, composition and mobility) characteristics of simple molecular aqueous fluids, brines or even aqueous solute-bearing fluids. Of these, aqueous solute-bearing fluids (with up to ~40% of dissolved rock components) are those expected to be circulating at colder HP-UHP conditions (High Pressure & Ultra-High Pressure, *i.e.*, in the deeper part of the forearc region and the subarc region; Frezzotti & Ferrando, 2015). Such chemical-physical characteristics in turn determine the effectiveness of such fluids in transferring rock-forming elements and redox potential from the down-going slab. They are among the least investigated due to difficulties in recognising them, in exhumated rocks, preserved within fluid inclusions (FI): post-entrapment processes (*e.g.*, solvent loss by diffusion or decrepitation and/or chemical reactions between host mineral and trapped fluid; Hall & Sterner, 1993) are likely to modify the chemical fingerprint of (UHP) fluid inclusions. Additionally, such fluids posed technical and scientific challenges to their thermodynamic modelling that have been overcome only recently (*i.e.*, electrolytic fluid thermodynamic modelling; Sverjensky *et al.*, 2014; Connolly & Galvez, 2018; Huang & Sverjensky, 2019).

Thus, this work aims to determine the composition of natural COHS fluids by combining direct (*i.e.*, fluid inclusions) and indirect (*i.e.*, thermodynamic modelling of electrolytic fluids) approaches, also assessing their respective reliability. Successively, it will need to explore the role of P, T and $f\text{O}_2$ on the solubility, speciation and redox state of C and S in the deep COHS fluids that potentially will metasomatize and regulate the redox state of the mantle wedge. This information has direct implications for volcanic explosivity, ore-forming processes and deep cycling of climate-forcing elements at convergent margins.

THERMODYNAMIC ANALYSIS OF HP-UHP FLUID INCLUSIONS: THE SOLUTE LOAD AND CHEMISTRY OF METAMORPHIC FLUIDS

In the first part of the thesis, I investigate fluid inclusions trapped within UHP clinopyroxene from a chemically simple impure UHP Ol-Cpx-Dol-Cal marble (DM675). The sample comes from the Brossasco-Isasca Unit (BIU), belonging to the UHP continental Dora-Maira Massif (Western Italian Alps; Fig. 1a), which reached 4.3 GPa and 730°C (Hermann, 2003; Castelli *et al.*, 2007; Groppo *et al.*, 2019) at 35 Ma (Gebauer *et al.*, 1997; Fig. 1b). An impure marble from a deeply subducted and exhumated continental unit can be used as a natural proxy of the processes affecting carbonate-dominated sediments subducted at subarc depths. Moreover, this sample preserves microstructural evidence of multiple carbonate dissolution-reprecipitation events during the prograde to peak evolution of the BIU (Ferrando *et al.*, 2017; Fig. 2).

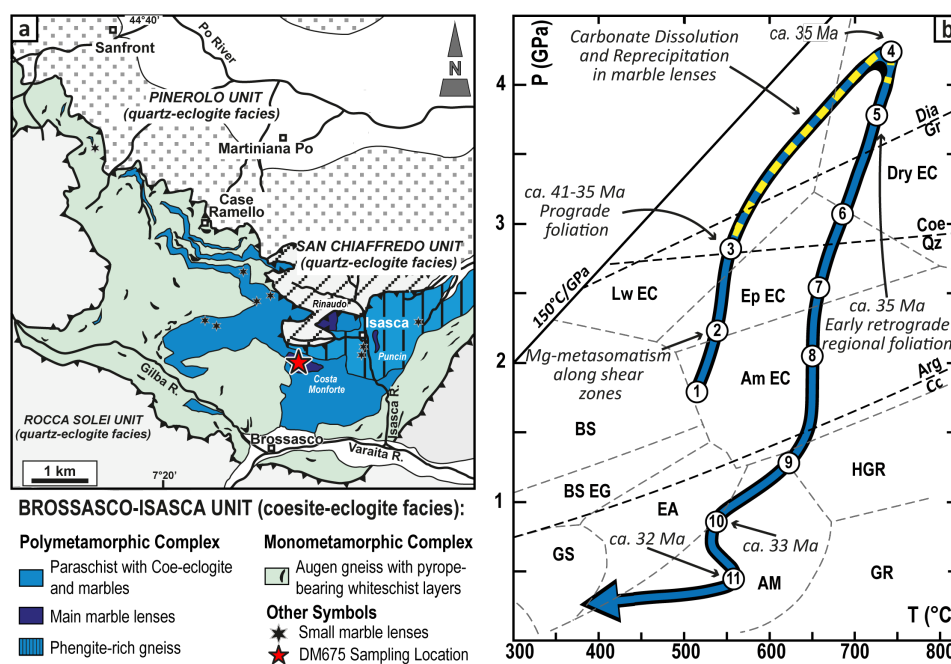


Fig. 1 - a) Simplified geologic map of the Brossasco-Isasca Unit modified from Ferrando *et al.* (2017). b) Alpine P-T-t-d path of the Brossasco-Isasca Unit inferred from previous studies (prograde path: Groppo *et al.*, 2019; peak and retrograde path: from Ferrando *et al.*, 2017 and references therein). The dashed yellow line indicates the P-T interval in which Ferrando *et al.* (2017) inferred the occurrence of carbonate dissolution and reprecipitation.

Primary fluid inclusions are observed within prograde-to-peak diopside (Fig. 2) and are defined as tri-phase multisolid fluid inclusions due to the occurrence, within them, of calcite + talc ± dolomite ± serpentine polymorphs ± Mg-calcite ± tremolite ± sulphide ± graphite and H₂O ± CH₄ ± N₂ (primary Type Ia, Ib, Ic and Id, characterised by an increasing amount and variety of included solids and correspondingly preserved fluid phases; Fig. 3a). They are also microstructurally associated to calcite or dolomite ± graphite mineral inclusions. Classical molecular-fluid thermodynamics is adequate to qualitatively describe the post-entrapment reactions between fluid inclusions and host diopside, showing how all the carbonate and silicate minerals can be step-daughter minerals (*i.e.*, included minerals produced by the reaction between an included fluid and the host mineral; Fig. 3a). Graphite and sulphide, instead, are true daughter minerals derived from C and S precipitation from the included fluid only at extreme solvent loss from the fluid inclusion. However, an electrolytic fluid model is necessary to describe quantitatively the chemical composition of the peak solute-bearing aqueous fluid (H₂O: 96.30 mol%/88.49 wt.%; solutes: 3.61 mol%/11.34 wt.%/2.08 mol/kg; other volatiles: 0.09 mol%/0.17 wt.%) generated by progressive rock dissolution. A comparison of the model fluid composition and the composition inferred from fluid inclusions clarifies the types and the extent of post-trapping chemical modification of the UHP fluid inclusions (Fig. 3b, c). Our data reveal that

the fluid-host reactions carry up to 42 mol% of host diopside component in the fluid inclusion bulk composition, whereas the fluid inclusion decrepitation and the water diffusion in the host diopside (through dislocations and/or micro-fractures) cause an H₂O loss ranging from 18 mol% upto 99 mol% (Fig. 3b). Applying these approaches, it is demonstrated that the most frequent and relevant post-entrapment process is H₂O loss, but also that some fluid inclusions did not experience post-entrapment fluid-host modification and, thus, preserve the original fluid geochemistry. Moreover, it is also shown that novel electrolytic fluid thermodynamic modelling is capable to reproduce naturally occurring UHP solute-bearing aqueous fluid composition.

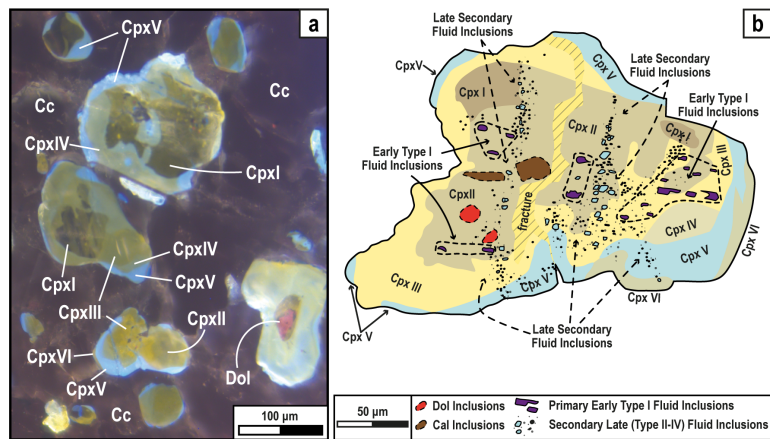


Fig. 2 - a) Cathodoluminescence (CL) photomicrographs of characteristics dissolution-reprecipitation related clinopyroxene zoning. b) Comprehensive sketch of a CL photomicrographs of a Cpx characterised by all six Cpx generations. The microstructural relationships between primary fluid inclusions, secondary fluid inclusions, carbonate inclusions and mineral zoning are outlined. Note that Type I fluid inclusions are present only in CpxII and CpxIII, whereas secondary fluid inclusions crosscut all Cpx generations. Solid carbonate inclusions are included only in Cpx II.

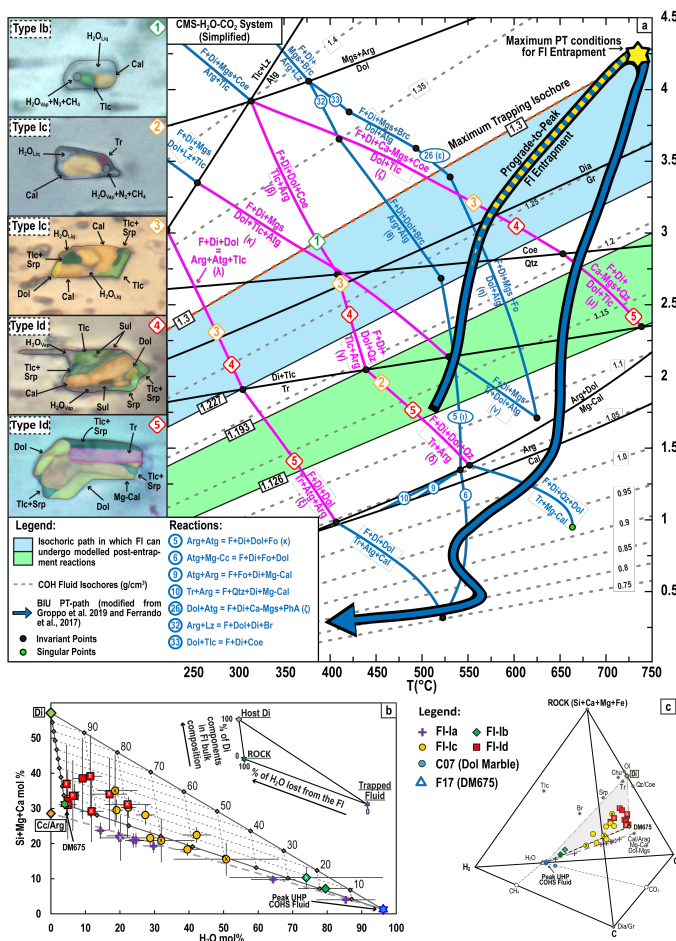


Fig. 3 - a) Simplified petrogenetic grid of the general system CMS-H₂O-CO₂ calculated to model post-entrapment reactions between host Di and included fluid. Pink lines are the reactions capable of reproducing the observed mineral association within Early Type I fluid inclusions. Blue lines are reactions that could have been active but whose products are not observed as a mineral association within Early Type I fluid inclusions. The selected FIs representative of the Type I FI re-equilibration stages are reported in the sketched photomicrographs on the left part of the figure. Correspondence between stepdaughter minerals in the photomicrographs and the producing reactions are visualised with coloured numbers in diamonds. Dotted lines are isochores calculated for a COH fluid composed by H₂O = 99.95 mol%, CO₂ = 0.05 mol%. b) Discrimination diagram showing the measured FI composition, and relative estimation error, in terms of molar H₂O and Si+Ca+Mg, to highlight the relationships between the fluid inclusion modified composition and the host Di, the original COHS peak fluid composition and the bulk-rock composition (DM675). This triangle highlights the amount of Di contamination within fluid inclusions and the degree of H₂O loss from the same fluid inclusions. c) Tetrahedron describing the chemical relationships between reconstructed fluid inclusion compositions, modelled peak fluid, bulk-rock, and mineral phases characterising the studied system in terms of system components. The grey triangle represents the plane whose vertices are the modelled fluid, the bulk rock, and the host Di, because this plane contains the measured fluid inclusion compositions.

CHEMICAL EVOLUTION OF THE CARBONATIC CFMS-COHS SYSTEM DURING COLD SUBDUCTION AS A FUNCTION P-T- fO_2

Demonstrating the effectiveness of electrolytic fluid thermodynamic modelling in reproducing naturally occurring UHP solute-bearing aqueous fluid composition, allows for an in-depth modelling of the effect of P-T- fO_2 , and also whether some metamorphic reactions exert, or not, any meaningful influence, on the speciation and composition of solute-bearing COHS aqueous fluids. Thermodynamic modelling is based on the impure marble composition DM675, using the sample's microstructure and inclusion-hosted redox constraints to validate the model. This led to the estimation of the DM675 fO_2 : a reduced marble with a redox state in the range $-2.2 < \Delta FMQ$ fO_2 log units < -1.9 (FMQ: Fayalite-Magnetite-Quartz oxygen buffer). Equilibrium metacarbonate phase relations show that, along the cold BIU subduction PT-path, with increasing oxygen fugacity, diamond and graphite are replaced by dolomite ~ 2 - 2.5 fO_2 log units before sulphide oxidizes to anhydrite (Fig. 4a). This redox-dependent decoupled stability of C and S minerals is the predisposing condition for the decoupled compositional and redox behaviour of carbon and sulphur in subduction fluids at the same P-T- fO_2 conditions. Equally important reactions are the discontinuous brucite-dehydration and the continuous antigorite-dehydration (Fig. 4a). These produce an interstitial aqueous fluid at forearc conditions that gradually dissolves the host rock and that, at subarc conditions (and assuming a closed system behaviour), becomes a solute-bearing aqueous fluid (solute load of 9-18 wt.%, depending on the system's redox state).

Fluid bulk composition is characterised by a generalised increase of all components as P and T increase due to continuous rock dissolution. Between $\Delta FMQ+2$ and $\Delta FMQ-2$, Mg, Si and Fe (due to its extremely low abundance in the investigated chemical system) solubility is barely affected by different redox conditions (Fig. 4b, c, e), while the ones of Ca, S and C are strongly influenced (Fig. 4d, f, g). Ca and S are more soluble at oxidised conditions above FMQ, while C roughly doubles its solubility at reduced conditions below $\Delta FMQ-1$.

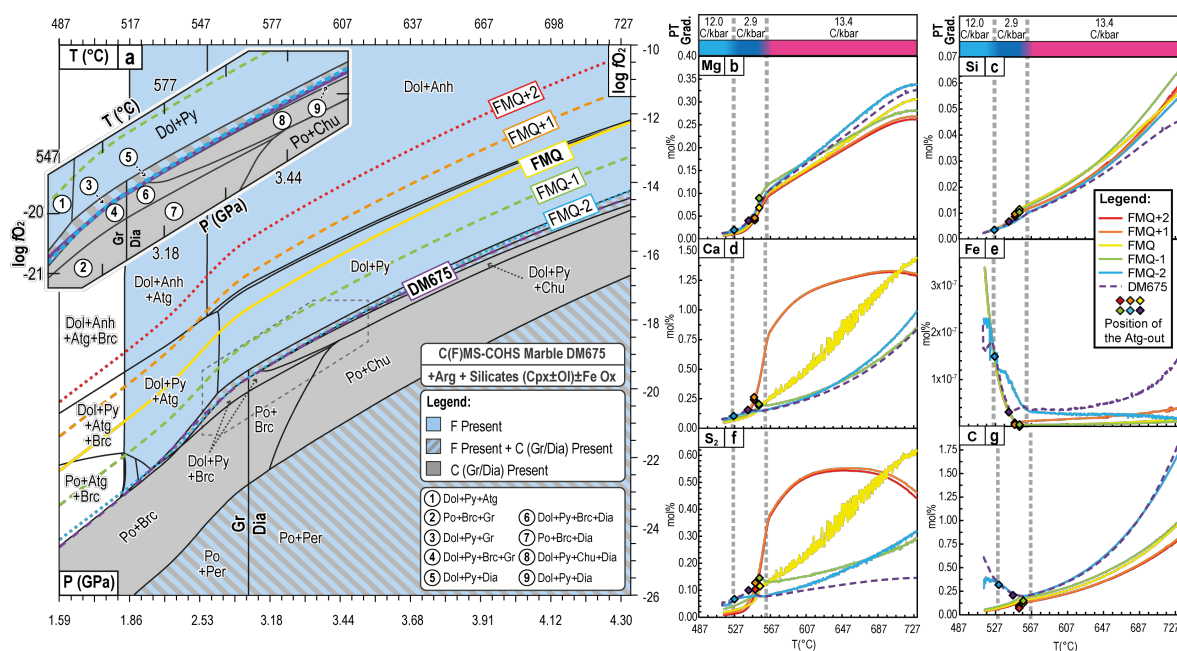


Fig. 4 - a) Simplified P-T- fO_2 compositional phase diagram along the BIU PT-path, for DM675 bulk composition, where only phase boundaries relevant to C and S redox-sensitive mineral phases and hydrated mineral phases are present. The coloured dotted and continuous lines indicate the position at which the fluid chemistry has been evaluated and reported in b-g) plots showing the bulk composition of the fluid in terms of system components and as a function of P-T- fO_2 . The dashed grey lines mark changes in the PT gradient used for calculation. The colour coding at the top of b and c corresponds to the colours used in Fig. 7e.

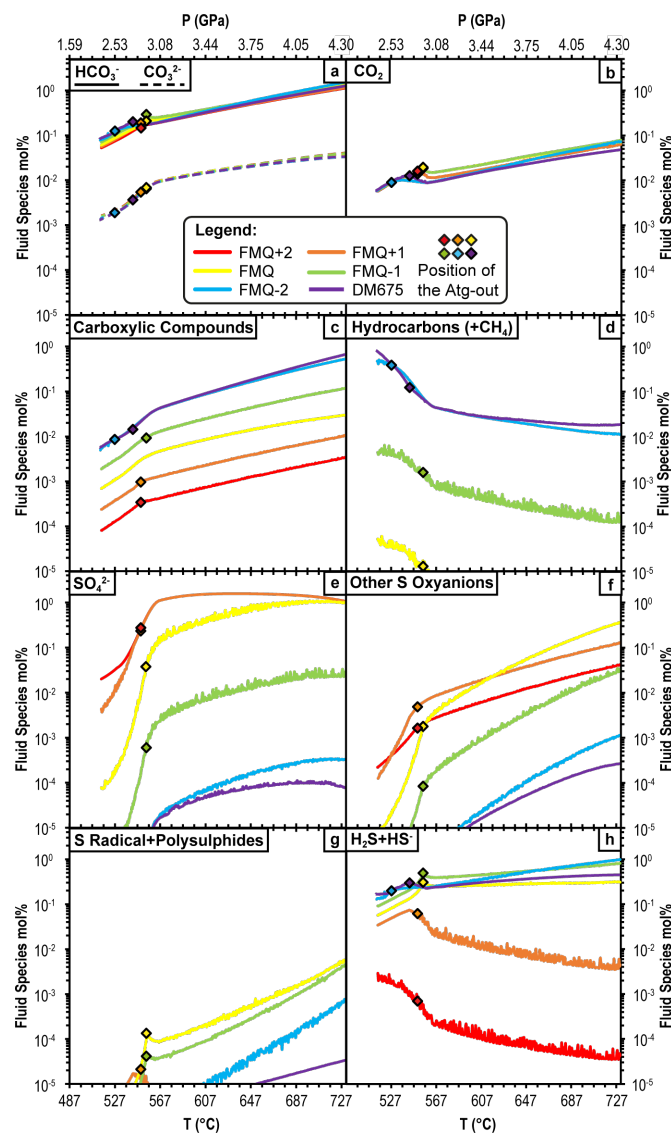


Fig. 5 - Chemistry of aqueous solute-bearing COHS fluid at increasing P/T conditions and different carbonate system redox states. For the sake of conciseness and simplicity, only the state of major C and S species groups, as a function of P-T and fO_2 , are reported. To improve the legibility of C and S speciation data, the species have been grouped according to chemical similarities.

The calculated fluid speciation, even for a chemically simple system as the one chosen here, is complex and articulated. For simplicity, here only C and S species are reported, but the fluid contains also various aqueous silica species, hydroxides, single element ions, alcohols, SO_2 , CO, H_2 and H^+ . Among major C species, C^{+4} ones (*i.e.*, HCO_3^- , CO_3^{2-} and CO_2) are mostly immune to differences in the system's redox state: the relatively infinite carbonate abundance (Arg±Dol) in the mineral assemblage buffers their abundance in the fluid (Fig. 5a, b). Above FMQ-1 they are the dominant form of C in the fluid. On the other hand, all the other C species characterised by C with a variably reduced valence state (VS; $-4 \leq VS < +3$) are strongly influenced by different system's redox states. Carboxylic compounds increase their abundance from oxidised to reduced condition by nearly 3 orders of magnitude, reaching similar abundances to those of C^{+4} species. Hydrocarbons show an even more dramatic change in their abundance with varying system's redox states, becoming irrelevant at FMQ and above. S speciation is more linearly correlated with the system redox state than C speciation. At oxidised conditions (*i.e.*, $\Delta FMQ+2$ and $\Delta FMQ+1$), anhydrite dissolution stabilises SO_4^{2-} species in the fluid with a minor contribution of other oxyanions

(e.g., HSO_3^-). At FMQ pyrite dissolves by disproportionation into fully oxidised SO_4^{2-} , intermediate S oxyanions and S radical (S_3^-) and fully reduced $\text{H}_2\text{S}+\text{HS}^-$ species. Conversely, pyrite, at reduced conditions (i.e., lower than $\Delta\text{FMQ}-1$), predominantly dissolves as sulphide species $\text{H}_2\text{S}+\text{HS}^-$. The calculated fluid speciation shows, for the first time, how P, T and most importantly $f\text{O}_2$ are determinant factors in C and S mobilisation in subduction-zone fluids and that drastic changes in dominant fluid species can occur across short $f\text{O}_2$ intervals (i.e., within 1 or less log unit of $f\text{O}_2$).

The fluid composition and speciation are chiefly influenced by changes in intensive parameters. However, locally the effect of a fundamental dehydration is also recorded by the fluid: the antigorite-dehydration. More specifically, in correspondence of the Atg-out, a peculiar local increase, followed by a sudden decrease in fluid species and corresponding rock-forming elements is observed (Fig. 5). This behaviour is directly tied to the role of the Atg-dehydration in producing oxidising or reducing fluids, which is a subject of heated debate in the literature over the last 8 years (e.g., Debret & Sverjensky, 2017; Vitale Brovarone *et al.*, 2017; Piccoli *et al.*, 2019; Maurice *et al.*, 2020). Electrolytic fluid modelling offers the possibility to compute an overlooked, but fundamental, parameter for fluid-bearing systems: the pH. Additionally, the difference between the neutral pH and the actual fluid pH ($\Delta\text{pH} = \text{pH} - \text{pH}_{\text{NEUTRAL}}$; Galvez *et al.*, 2016) better describes the a_{H^+} , which describes changes in the activity and ionisation constant of H_2O . The contoured ΔpH values in Fig. 6 show how the fluid phase becomes more acidic toward the end of the Atg-dehydration, irrelevant of the redox state of the system, but still with reduced conditions being more acidic than oxidised one. This explains the local increase in some fluid species and rock-forming elements. The lack of permanent changes in the abundance of redox-sensitive fluid species after the Atg-out suggests that the redox state of the fluid in rock-buffered systems is imposed by the rock and not by this specific reaction, supporting the recent global evaluation of Evans & Frost (2021). Nevertheless, the possibility that fluid-involving metamorphic reactions should be capable of changing the fluid pH and thus the efficiency of mineral dissolution in a subducting slab is highlighted by employing electrolytic fluid thermodynamic modelling techniques.

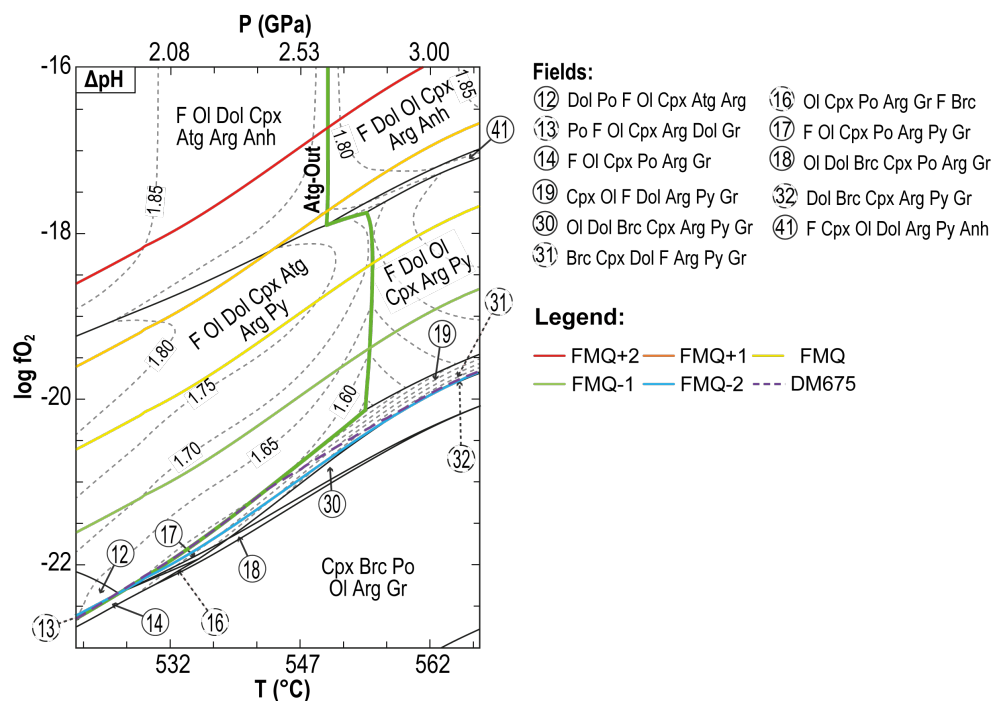


Fig. 6 - Enlargement of the calculated P-T- $f\text{O}_2$ compositional phase diagram (Fig. 4a) around the Atg-out, with a contouring for $\Delta\text{pH} = \text{pH} - \text{pH}_{\text{NEUTRAL}}$ (Galvez *et al.*, 2016).

To better evaluate solely the effect of fO_2 on C and S solubility in aqueous subduction-zone fluids, equilibrated with carbonate sediments, the calculated rock and fluid model has been evaluated at fixed PT conditions but with variable fO_2 . Two representative locations on the PT path have been chosen:

- point α (2.53 GPa and 547°C) is located at forearc conditions and is placed at roughly 10°C and 0.2 GPa before the Atg-out, allowing the evaluation of the fluid chemistry at the stage of maximum fluid production.

- point β (4.22 GPa and 712°C) close to the metamorphic peak in the subarc region, allowing the evaluation of the effect of prolonged prograde rock dissolution on the fluid chemistry that might be released below a volcanic arc.

C and S solubility increases with increasing P and T by a factor of ~ 6 and between ~ 4 and ~ 7.5 for C and S (the latter depending on the system fO_2) from the forearc to the subarc, respectively. However, the system fO_2 determines what C and S mineral phases are stable and it's the solubility of each phase that controls the abundance (and speciation) of such elements within the fluid. C is more soluble at reduced conditions by a factor of ~ 2 (Fig. 7a, b). This increase is related to the presence, on top of nearly constant C^{+4} species, of variably reduced species like CH_4 (and other hydrocarbons in the forearc) and formate or propanoate (i.e., organic carboxylic compounds characterised by having multiple C atoms with different and intermediate VS within the same molecule, e.g., propanoate: $C^{-3}H^3C^{-2}H^2C^{+3}OO^-$). These additional species are related to the presence of graphite/diamond in the mineral assemblage and implies the presence of the whole and continuum range of C valence states within the fluid phase (Fig. 7a, b).

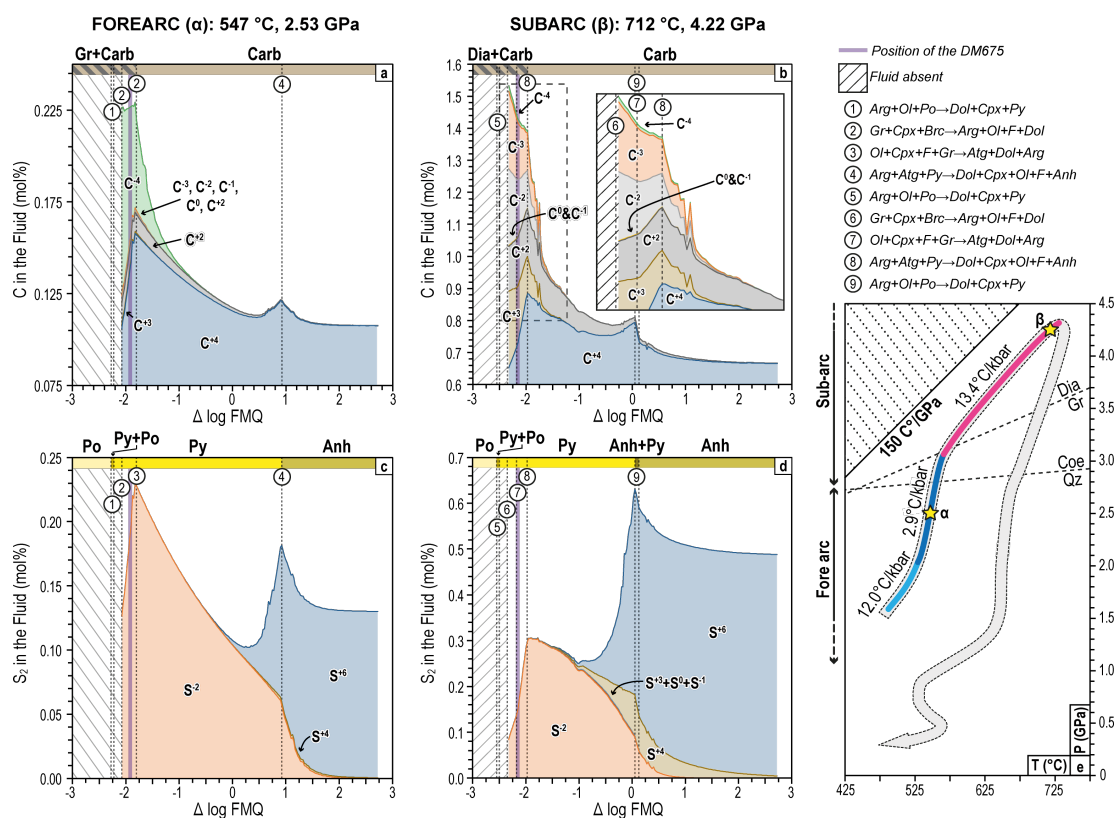


Fig. 7 - a-d) Variation of carbon and sulphur abundance in the fluid as a function of fO_2 in the forearc and subarc region. Moreover, is also shown the cumulative abundance of carbon and sulphur subdivided between all their possible valence states present in the fluid calculated from the fluid speciation. In violet is reported the position of the DM675 proxy sample. e) BIU PT-path where the three segments in which the PT path has been subdivided for calculation purpose.

Sulphur, on the other hand, has a more heterogeneous behaviour dictated by changes in pyrite solubilisation process at changing fO_2 conditions (shifting from simple dissolution by reduction to dissolution by

disproportionation) and then by anhydrite solubility. At forearc conditions, S is slightly more soluble at reduced conditions, but this is strongly dependent on the proximity of the system state to any redox-controlled reactions like the oxidation of pyrite to anhydrite (Fig. 7c, d). Conversely, at subarc depths anhydrite dissolution boost S solubility at oxidised conditions (compared to reduced one) by a factor of ~2. Like C, as the system is equilibrated at higher P and T, S-species with an intermediate VS (e.g., S⁺⁴) appear at intermediate redox conditions.

The presented results have overarching implications. Fluid inclusions and novel thermodynamic modelling using electrolytic fluid models are complementary, mutually supporting, and reliable tools to investigate the chemistry of HP-UHP subduction-zone fluids. C and S speciation calculated with electrolytic fluid models (i.e., comprising species like - but not limited to -, CO₂, CO₃²⁻, HCO₃⁻, Ca(HCO₃)⁺, HCOO⁻, C₃H₅O₂⁻, C₂H₆, C₃H₈, CH₄, SO₄²⁻, CaSO_{4,aq}, HSO₄⁻, HSO₃⁻, S₂O₃²⁻, S₃⁻, H₂S and HS⁻) moves away from the simpler speciation predicted by classical molecular fluid models (only CO₂, CO, CH₄, SO₂ and H₂S), leading to the depiction of a more realistic HP-UHP fluid composition. Considering this kind of data changes the effectiveness of aqueous fluids (now solute-bearing aqueous fluids) in triggering the mantle wedge metasomatism and oxidation, and the related magmatism, ore-forming processes and element cycling that take place at convergent margins.

REFERENCES

- Ballhaus, C. & Frost, B.R. (1994): The generation of oxidized CO₂-bearing basaltic melts from reduced CH₄-bearing upper mantle sources. *Geochim. Cosmochim. Ac.*, **58**, 4931-4940.
- Castelli, D., Rolfo, F., Groppo, C., Compagnoni, R. (2007): Impure marbles from the UHP Brossasco-Isasca Unit (Dora-Maira Massif, western Alps): evidence for Alpine equilibration in the diamond stability field and evaluation of the X (CO₂) fluid evolution. *J. Metamorph. Geol.*, **25**, 587-603.
- Connolly, J.A. & Galvez, M.E. (2018): Electrolytic fluid speciation by Gibbs energy minimization and implications for subduction zone mass transfer. *Earth Planet. Sc. Lett.*, **501**, 90-102.
- Debret, B. & Sverjensky, D.A. (2017): Highly oxidising fluids generated during serpentinite breakdown in subduction zones. *Sci. Rep.*, **7**, 1-6.
- Evans, K.A. & Frost, B.R. (2021): Deserpentinization in subduction zones as a source of oxidation in arcs: A reality check. *J. Pet.*, **62**, 1-32.
- Facq, S., Daniel, I., Montagnac, G., Cardon, H., Sverjensky, D.A. (2014): In situ Raman study and thermodynamic model of aqueous carbonate speciation in equilibrium with aragonite under subduction zone conditions. *Geochim. Cosmochim. Ac.*, **132**, 375-390.
- Ferrando, S., Groppo, C., Frezzotti, M.L., Castelli, D., Proyer, A. (2017): Dissolving dolomite in a stable UHP mineral assemblage: Evidence from Cal-Dol marbles of the Dora-Maira Massif (Italian Western Alps). *Am. Mineral.*, **102**, 42-60.
- Frezzotti, M.L. (2019): Diamond growth from organic compounds in hydrous fluids deep within the Earth. *Nat. Commun.*, **10**, 1-8.
- Frezzotti, M.L. & Ferrando, S. (2015): The chemical behavior of fluids released during deep subduction based on fluid inclusions. *Am. Mineral.*, **100**, 352-377.
- Frezzotti, M.L., Selverstone, J., Sharp, Z.D., Compagnoni, R. (2011): Carbonate dissolution during subduction revealed by diamond-bearing rocks from the Alps. *Nat. Geosci.*, **4**, 703-706.
- Frost, D.J. & McCammon, C.A. (2008): The redox state of Earth's mantle. *Ann. Rev. Earth Planet. Sci.*, **36**, 389-420.
- Galvez, M.E., Connolly, J.A., Manning, C.E. (2016): Implications for metal and volatile cycles from the pH of subduction zone fluids. *Nature*, **539**, 420-424.
- Gebauer, D.H.P.S., Schertl, H.P., Brix, M., Schreyer, W. (1997): 35 Ma old ultrahigh-pressure metamorphism and evidence for very rapid exhumation in the Dora Maira Massif, Western Alps. *Lithos*, **41**, 5-24.
- Groppo, C., Ferrando, S., Gilio, M., Botta, S., Nosenzo, F., Balestro, G., Festa, A., Rolfo, F. (2019): What's in the sandwich? New P-T constraints for the (U)HP nappe stack of southern Dora-Maira Massif (Western Alps). *Eur. J. Mineral.* **31**, 665-683.
- Hall, D.L. & Sterner, S.M. (1993): Preferential water loss from synthetic fluid inclusions. *Contrib. Mineral. Petr.*, **114**, 489-500.
- Hermann, J. (2003): Experimental evidence for diamond-facies metamorphism in the Dora-Maira massif. *Lithos*, **70**, 163-182.
- Huang, F. & Sverjensky, D.A. (2019): Extended Deep Earth Water Model for predicting major element mantle metasomatism. *Geochim. Cosmochim. Ac.*, **254**, 192-230.

- Kagoshima, T., Sano, Y., Takahata, N., Maruoka, T., Fischer, T.P., Hattori, K. (2015): Sulphur geodynamic cycle. *Sci. Rep.*, **5**, 1-6.
- Li, J.L., Schwarzenbach, E.M., John, T., Ague, J.J., Tassara, S., Gao, J., Konecke, B.A. (2021): Subduction zone sulfur mobilization and redistribution by intraslab fluid-rock interaction. *Geochim. Cosmochim. Ac.*, **297**, 40-64.
- Malusà, M.G., Frezzotti, M.L., Ferrando, S., Brandmayr, E., Romanelli, F., Panza, G.F. (2018): Active carbon sequestration in the Alpine mantle wedge and implications for long-term climate trends. *Sci. Rep.*, **8**, 1-8.
- Maurice, J., Bolfan-Casanova, N., Demouchy, S., Chauvigne, P., Schiavi, F., Debret, B. (2020): The intrinsic nature of antigorite breakdown at 3 GPa: Experimental constraints on redox conditions of serpentinite dehydration in subduction zones. *Contrib. Mineral. Petr.*, **175**, 1-23.
- Piccoli, F., Hermann, J., Pettke, T., Connolly, J.A.D., Kempf, E.D., Duarte, J.V. (2019): Subducting serpentinites release reduced, not oxidized, aqueous fluids. *Sci. Rep.*, **9**, 1-7.
- Plank, T. & Manning, C.E. (2019): Subducting carbon. *Nature*, **574**, 343-352.
- Sverjensky, D.A., Harrison, B., Azzolini, D. (2014): The dielectric constant and the solubilities of quartz and corundum to 60 kb and 1200 °C. *Geochim. Cosmochim. Ac.*, **129**, 125-145.
- Taylor, W.R. & Green, D.H. (1988): Measurement of reduced peridotite-COH solidus and implications for redox melting of the mantle. *Nature*, **332**, 349-352.
- Vitale Brovarone, A.V., Martinez, I., Elmaleh, A., Compagnoni, R., Chaduteau, C., Ferraris, C., Esteve, I. (2017): Massive production of abiotic methane during subduction evidenced in metamorphosed ophicarbonates from the Italian Alps. *Nat. Commun.*, **8**, 14134.
- Walters, J.B., Cruz-Uribe, A.M., Marschall, H.R. (2020): Sulfur loss from subducted altered oceanic crust and implications for mantle oxidation. *Geochem. Perspect. Lett.*, **13**, 36-41.